# Electronic, optical, and surface properties of PtSi thin films

H. Bentmann,[1] Alexander A. Demkov,[1,*] R. Gregory,[2] and S. Zollner[3]
[1]*Department of Physics, The University of Texas at Austin, Austin, Texas 78712, USA*
[2]*Freescale Semiconductor, Inc., Tempe, Arizona 85284, USA*
[3]*Freescale Semiconductor, Inc., Hopewell Junction, New York 12533, USA*
(Received 7 February 2008; revised manuscript received 9 September 2008; published 3 November 2008)

We report a theoretical and experimental study of thin Pt silicide films. Employing density-functional theory, we investigate the electronic structure, bonding, and optical properties of PtSi and $Pt_2Si$. Additionally, we calculate surface energies for various orientations and terminations of PtSi surfaces. Our results suggest that thermodynamics may play a role in the silicide formation. The complex dielectric function determined by spectroscopic ellipsometry exhibits non-Drude behavior and shows peaks, which are identified with interband transitions in the 5*d* manifold of platinum and compared with theory.

DOI: 10.1103/PhysRevB.78.205302 PACS number(s): 73.61.At, 71.55.Ak, 71.20.Be, 71.20.Nr

## I. INTRODUCTION

Transition-metal silicides have played an important role in the rapid development of microelectronic device technology.[1] They are used in complementary metal-oxide-semiconductor (CMOS) devices to form contacts between metal interconnects and source, drain, and gate silicon of the transistors. They offer important properties such as low resistivity and low contact resistance to Si as well as excellent process compatibility with the standard Si process technology. Recently, metal silicides have attracted renewed attention and they are a current research topic in the semiconductor industry.[2,3] Present issues are, for example, NiSi contacts in CMOS devices of the 32 and 22 nm nodes and low-Ohmic-resistance PtSi contacts in *p*-channel metal-oxide-semiconductor (PMOS) field-effect transistors (FETs). Most transition-metal silicides, i.e., NiSi or $CoSi_2$, have Schottky barrier heights of about 0.5 eV for both *n*-type and *p*-type silicon as their Fermi level aligns with the center of the Si band gap. The Schottky barrier height determines the specific contact resistivity between the silicide (metal) and silicon. This contact resistance currently amounts to a quarter of the total parasitic resistance in the metal-oxide-semiconductor field-effect transistors (MOSFETs) and will clearly only rise as scaling continues.[4] Thus, identifying materials that are able to lower the contact resistance is important.[5] PtSi is one of the candidates due to its relatively low Schottky barrier of only 0.3 eV to *p*-type Si,[6] and excellent thermal stability.[7] We recently reported the integration of PtSi contacts into a 65 nm CMOS process flow and showed improved PMOS device characteristics.[8,9]

In addition to its importance in technology, PtSi is of interest from the fundamental scientific point of view as a material that is neither well described with the picture of a typical metal nor that of a typical semiconductor. The bulk electronic structure of PtSi and the bond character between Pt and Si were until recently poorly understood. In a series of three publications Klepeis and co-workers[10–12] presented a comprehensive theoretical and experimental study on the electronic structure of bulk PtSi and also $Pt_2Si$, revealing interesting insights. In addition, the characterization of the thin-film growth of PtSi, which will be explained below, has been the subject of several studies.[13,14] Stark *et al.*[14] reported measurements of the optical constants of the constituent phases Pt, $Pt_2Si$, and PtSi in the range between 1.5 and 4.5 eV. In a previous publication we calculated surface energies and work functions for PtSi surfaces as well as the Schottky barrier height at the Si(001)/PtSi(001) interface.[6]

The main goal of the present paper is to establish a relation between calculated properties, such as band structure and surface energy (governed by atomic geometry and composition), and experimental observables, such as dielectric function and preferred crystal-growth direction of PtSi films on Si. For this purpose the x-ray-diffraction and ellipsometry data of a 33 nm PtSi film are collected, analyzed, and compared with the results of first-principles calculations. It should be noted that though we do not model the Si/PtSi explicitly in this paper, the results should provide a reasonable approximation to consider experimental data. Our previous theoretical model of this interface resulted in the Schottky barrier height in good agreement with experiment.[6] The rest of the paper is organized as follows. First we present the experimental methods we employed and discuss the growth of PtSi on a Si substrate. We also summarize the experimental results we obtained. Then we provide a short summary of the computational details of our theoretical work. Thereafter, we present the analysis of bulk PtSi and $Pt_2Si$ in terms of crystal structure as well as electronic and optical properties, and compare the latter with the ellipsometry data. We report on surface energies and work functions, focusing on the Si-terminated PtSi surfaces. We conclude with the finding of an unusual reconstruction of the (101) Si-terminated surface of PtSi.

## II. EXPERIMENTAL RESULTS

Pt-Si films were formed by annealing of 17 nm of Pt deposited on Si [wafer A annealed at 300 °C for 10 s; wafer B annealed at 600 °C for 30 s; both are (001) oriented]. Figure 1 schematically shows five steps involved in the preparation of a PtSi film on a Si substrate: annealing causes Pt atoms to diffuse into the Si substrate, forming $Pt_2Si$. The depletion of the Pt layer ends this process and a layer of pure $Pt_2Si$ is formed. Further annealing causes Si atoms to migrate

 ©2008 The American Physical Society

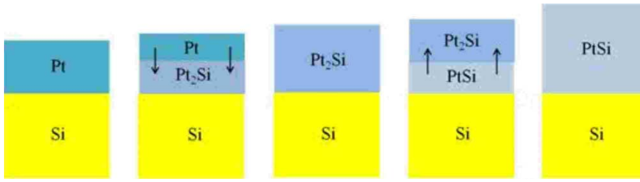


FIG. 1. (Color online) Schematic figure illustrating the sequential formation process of PtSi on a Si substrate. After deposition of the Pt layer on the Si substrate, annealing causes Pt atoms to migrate into the substrate, forming $Pt_2Si$. At higher temperatures Si atoms start migrating into the $Pt_2Si$ film, forming PtSi.

into the $Pt_2Si$ layer, forming PtSi. A reaction front (the interface between PtSi and $Pt_2Si$) moves upward until the complete PtSi layer is formed. It is important to note that two diffusion processes, Pt into Si and Si into $Pt_2Si$, happen sequentially. Not until the full $Pt_2Si$ film is established does the PtSi formation set in. The thickness of the as-deposited pure Pt film in our case is about 17 nm ($\pm 5\%$), as determined by a combination of Rutherford backscattering, x-ray fluorescence, and x-ray reflectance. More precisely, the pure Pt film would be about 17 nm thick if it was deposited on oxide. Since this film was deposited on Si, some Pt reacts with the Si surface during deposition, which leads to a multilayer structure (thicker than 17 nm, but less dense) consisting of pure Pt on a metal-rich Pt-Si interfacial layer. After annealing to form monosilicide PtSi, the film thickness is about 33 nm. X-ray-diffraction spectra shown in Fig. 2 are acquired in a powder diffractometer in $\theta$-$2\theta$ mode (where the detector moves at twice the angular velocity of the sample) using a Cu $K\alpha$ rotating anode source (wavelength: 1.54 Å). Peak assignments are performed based on the ICDD database, card no. 07-0251.

The complex pseudodielectric functions from 0.8 to 6.6 eV for two Pt-Si films (produced by annealing at different temperatures as above) are shown in Fig. 3. The data were acquired on a variable-angle-of-incidence rotating-analyzer

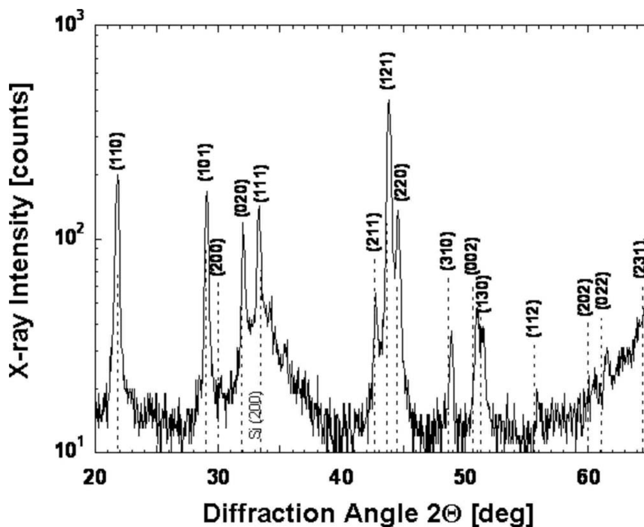


FIG. 2. X-ray-diffraction spectrum ($\theta/2\theta$) for a 33-nm-thick film of PtSi. Several orthorhombic PtSi diffraction peaks are indexed.

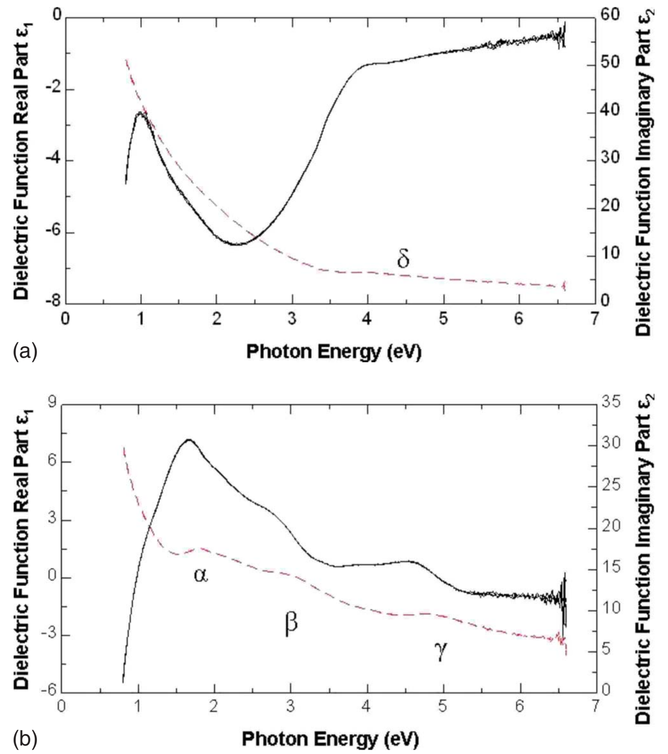


FIG. 3. (Color online) Complex pseudodielectric functions measured by spectroscopic ellipsometry for (a) wafer A ($Pt_2Si$) and (b) wafer B (PtSi). The Drude behavior is superposed by contributions due to interband transitions. The Greek letters label the interband transitions for comparison with theory (Fig. 11).

spectroscopic ellipsometer (at three angles of incidence, 65°, 70°, and 75°) equipped with a computer-controlled Berek waveplate compensator. The real part is shown by the solid (black) lines and the imaginary part by the dashed (red) lines. For an infinitely thick film without native oxide, the pseudodielectric function $\langle \varepsilon \rangle$ would be the same as the dielectric function $\varepsilon$ of the material. In our case, the spectra are influenced to a small extent by a thin film of native oxide and by the Si substrate since the film thickness is only about twice the optical penetration depth (20 nm) in the infrared spectral region. Nevertheless, the experimental spectra are expected to show similar features as the dielectric function of platinum silicide. The data are dominated by the Drude divergence in the infrared (imaginary part goes to infinity, real part to negative infinity), superimposed by peaks caused by optical interband transitions, which will be discussed below.

## III. COMPUTATIONAL DETAILS

Our theoretical calculations on PtSi, $Pt_2Si$, Pt, and Si are performed within the generalized gradient approximation (GGA) to density-functional theory (DFT) with a plane-wave basis using the VASP code.[15] We employ projector augmented wave (PAW) pseudopotentials for both species.[16,17] Exchange and correlation are treated within the Perdew-Burke-Enzerhof (PBE) form of the GGA functional.[18] The plane-wave expansion is restricted by a kinetic-energy cutoff of 245 eV. Forces are calculated via the method of Hellmann

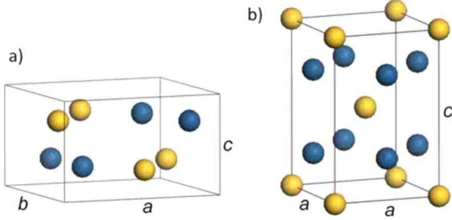


FIG. 4. (Color online) (a) The orthorhombic unit cell of bulk PtSi and (b) the body-centered-tetragonal unit cell of bulk $Pt_2Si$ (b). Dark (light) balls represent Pt (Si) atoms. Lattice constants and internal parameters are given in Tables I and II, respectively.

and Feynman and minimized by employing the conjugate-gradient technique. The structures are relaxed until the forces on all atoms are below 20 meV/Å. In bulk calculations we employ dense $k$-point grids of $13\times13\times17$ (PtSi), $17\times17\times13$ ($Pt_2Si$), $13\times13\times13$ (Pt), and $8\times8\times8$ (Si). The total energy is converged to $10^{-6}$ eV/cell.

The absorption coefficient $\varepsilon_2$ of PtSi and $Pt_2Si$ is calculated with the CASTEP code.[19] $\varepsilon_2$ is the imaginary part of the complex dielectric function $\varepsilon=\varepsilon_1+i\varepsilon_2$. We use 144 $k$ points in the irreducible wedge of the Brillouin zone (BZ) for PtSi and 192 for $Pt_2Si$. Within the DFT-GGA the contributions to $\varepsilon_2$ due to interband transitions can be calculated according to the usual expression[20]

$$\varepsilon_2(\boldsymbol{q}\to 0,\hbar\omega)=\frac{2\pi}{\Omega\varepsilon_0}\sum_{nk,v,c}|\langle\psi^c_{nk}|\boldsymbol{u}\cdot\boldsymbol{r}|\psi^v_{nk}\rangle|^2\delta(E^c_{nk}-E^v_{nk}-\hbar\omega), \tag{1}$$

where $\boldsymbol{u}$ is the unit vector defining the polarization of the incident electromagnetic wave and $\omega$ is the frequency of the incoming photons. $\psi^{c,v}_{nk}$ are the unoccupied and occupied Kohn-Sham wave functions, respectively, and $E^{c,v}_{n\mathbf{k}}$ are the corresponding one-electron energies. The calculations are performed for unpolarized light. We accounted for intraband transitions by employing an empirical Drude term.

## IV. BULK PROPERTIES OF PtSi AND $Pt_2Si$

### A. Crystal structure

PtSi crystallizes in the primitive orthorhombic structure in a MnP-type lattice with space group *Pnma* (No. 62 in the International X-Ray Tables).[21] Three lattice constants $a$, $b$, and $c$ define the primitive unit cell. In addition, four internal in-plane parameters $u_{Si}$, $v_{Si}$, $u_{Pt}$, and $v_{Pt}$ determine the positions of the four Pt atoms and the four Si atoms within the unit cell. The caption of Table II gives the atomic positions in terms of these parameters. In its $\alpha$ phase at $T<968$ K, $Pt_2Si$ adopts the body-centered-tetragonal crystal structure with the space group $I4/mmm$ (No. 139 in the International X-Ray Tables).[22] Two lattice constants $a$ and $c$ define the primitive unit cell. In Fig. 4 the crystal structures of both silicide phases are displayed. The lattice constants we calculated are summarized and compared to experimental values in Table I. The four internal parameters for PtSi are given in Table II. Overall we find agreement within 1.5%.

Additionally, Table I shows cohesive energies $E_{coh}$ of all elements and heats of formation $\Delta H_f$ for the two silicides. The agreement with the experimental values is reasonably good. In particular, unlike in Ref. 10, our calculation correctly identifies the heat of formation of $Pt_2Si$ to be larger than that of PtSi.

TABLE II. Experimental and calculated internal in-plane coordinates of PtSi. The values are given in direct coordinates. The Pt atoms are located at $[u_{Pt},v_{Pt},\frac{1}{4}]$, $[(\frac{1}{2}-u_{Pt}),(v_{Pt}-\frac{1}{2}),\frac{1}{4}]$, $[(1-u_{Pt}),(1-v_{Pt}),\frac{3}{4}]$, and $[(\frac{1}{2}+u_{Pt}),(\frac{3}{2}-v_{Pt}),\frac{3}{4}]$, while the Si atoms are located at $[u_{Si},v_{Si},\frac{1}{4}]$, $[(\frac{3}{2}-u_{Si}),(\frac{1}{2}+v_{Si}),\frac{1}{4}]$, $[(u_{Si}-\frac{1}{2}),(\frac{1}{2}-v_{Si}),\frac{3}{4}]$, and $[(1-u_{Si}),(1-v_{Si}),\frac{3}{4}]$.

| PtSi | $u_{Pt}$ | $v_{Pt}$ | $u_{Si}$ | $v_{Si}$ | Reference |
|---|---|---|---|---|---|
| Theor. | 0.193 | 0.995 | 0.583 | 0.178 | |
| Expt. | 0.1936 | 0.9945 | 0.5835 | 0.1784 | 21 |

### B. Electronic structure

In Fig. 5 we compare the band structures of PtSi and $Pt_2Si$ along high-symmetry lines in the BZ. The corresponding densities of states (DOSs) are presented in Fig. 6. For comparison we show the DOS of Pt as well. Figure 7 shows orbital-resolved partial densities of states (PDOSs) of the two silicides. As can be seen in Fig. 6 the DOSs of PtSi and $Pt_2Si$ at the Fermi level are about seven times lower than that of Pt, indicating the two silicides to be poor metals. The

TABLE I. Theoretical and experimental lattice constants, heats of formation, and cohesive energies for Si, Pt, PtSi, and $Pt_2Si$. The experimental standard heats of formation are given for $T=298.15$ K.

| Material | | $a$ (Å) | $b$ (Å) | $c$ (Å) | $E_{coh}$ (eV/atom) | $\Delta H_f$ (eV/atom) | Reference |
|---|---|---|---|---|---|---|---|
| Si | Theor. | 5.465 | | | 4.60 | | |
| | Expt. | 5.428 | | | 4.63 | | 23 |
| Pt | Theor. | 3.975 | | | 5.53 | | |
| | Expt. | 3.927 | | | 5.84 | | 23 |
| PtSi | Theor. | 5.983 | 5.653 | 3.633 | 5.73 | −0.67 | |
| | Expt. | 5.922 | 5.575 | 3.586 | 5.85 | −0.62 | 21 |
| $Pt_2Si$ | Theor. | 3.975 | | 5.996 | 5.94 | −0.72 | |
| | Expt. | 3.935 | | 5.910 | 6.08 | −0.64 | 22 |

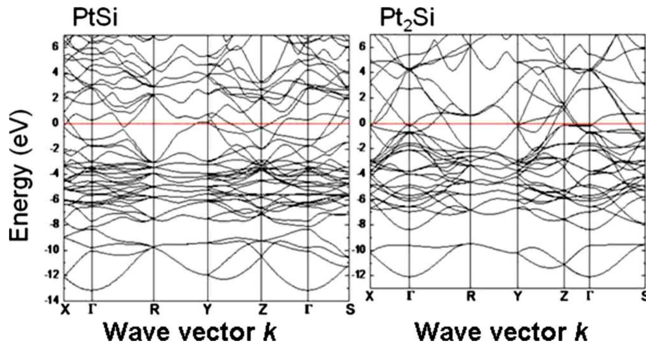


FIG. 5. (Color online) Bulk band structures along high-symmetry lines of PtSi and $Pt_2Si$. The dense manifolds of flatbands below the Fermi energy (red line) mainly arise from Pt 5*d* states. Pt atoms are shown with darker balls.

states at the Fermi energy mainly arise from Pt 5*d* states as evident from Fig. 7. While in the case of Pt the Fermi level lies near a DOS maximum due to the Pt 5*d* states, it lies near a DOS minimum in the case of PtSi and $Pt_2Si$ (Fig. 6). For PtSi the 5*d* manifold starts at about 3 eV below the Fermi energy $E_F$ and for $Pt_2Si$ at about 1.7 eV below $E_F$. This is due to the fact that the ratio between the number of *d* states and the number of electrons per unit cell is reduced to 77% (83%) for PtSi ($Pt_2Si$) when compared to Pt. This also explains why the 5*d* manifold lies deeper below the Fermi energy for PtSi than for $Pt_2Si$.

In Fig. 6 we further observe a prominent peak at the bottom of the valence band near −9.5 eV for both silicides. This peak has been reported for nearly every silicide and used to be associated with unhybridized Si 3*s* states, which were believed until recently to be insensitive to the transition metal–silicon bonding. However, in Fig. 7 we clearly see that for both silicides the Pt 5*d* states contribute almost an equal amount to the DOS peak as the Si 3*s* states. This is in agreement with the recent experimental and theoretical results,[8,11] suggesting that Si 3*s* states and Pt 5*d* states do mix at the bottom of the valence band and that the latter extend throughout the entire valence band instead of being localized.

### C. Nature of bonding in PtSi and $Pt_2Si$

The electronic structure of PtSi and $Pt_2Si$ explains why both are poor metals in terms of conductivity. It also allows for an investigation of the bond character by directly analyzing the valence charge density. In what follows we subtract the atomic valence charge densities from the calculated self-consistent densities with the intention to emphasize the charge transfer due to the crystal or bond formation:

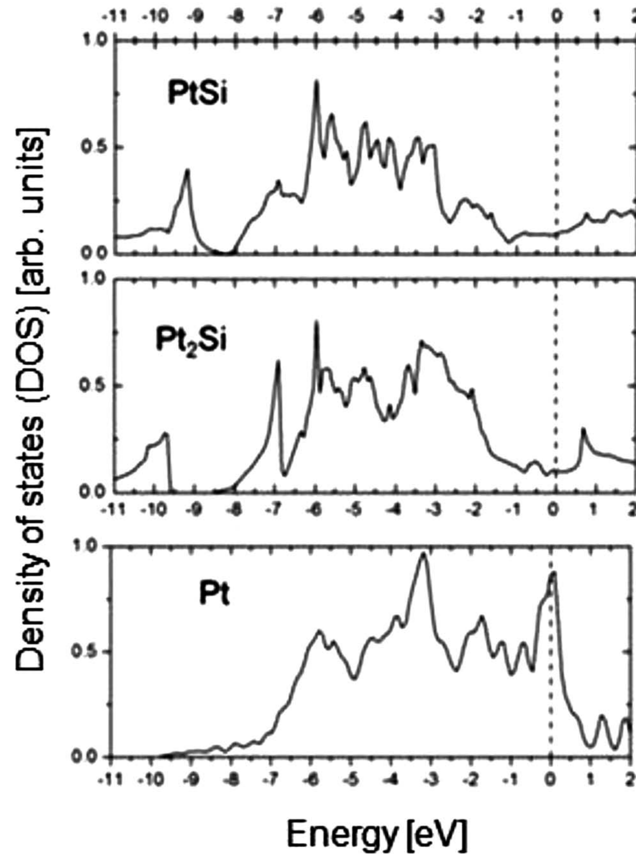


FIG. 6. Total DOSs of PtSi, $Pt_2Si$, and Pt. For Pt the Fermi energy (dashed line) lies right at the top of the high-density region of the 5*d* manifold. Consequently the DOS at the Fermi level is high, a typical property of a good metal. In the cases of the two silicides, the Fermi level "misses" the 5*d* manifold, which results in a low DOS at the Fermi energy. This suggests the two silicides to be rather poor metals.

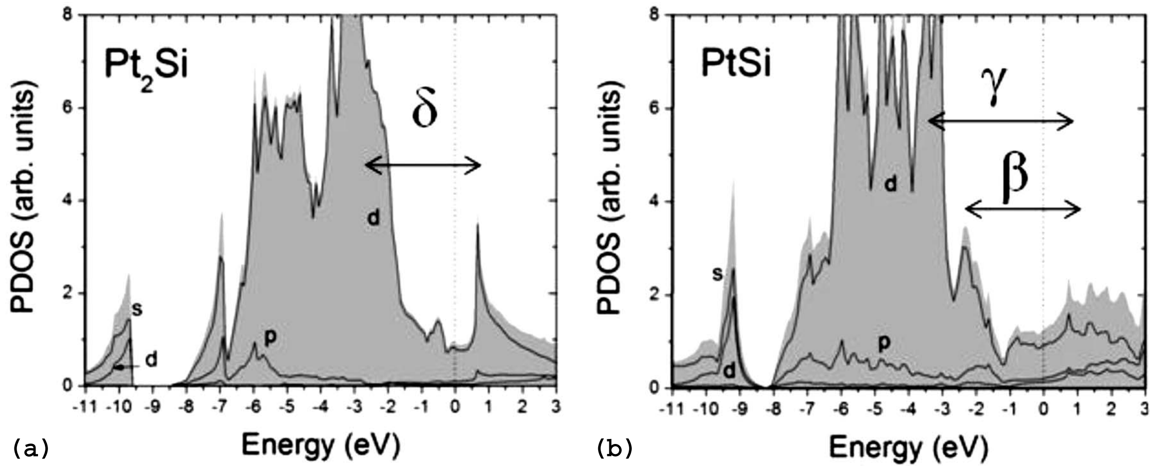


FIG. 7. PDOSs of (a) PtSi and (b) $Pt_2Si$. The Fermi energy is indicated with a dashed line. The platinum 5*d* states extend over the entire valence band in the case of both silicides. The peaks at the bottom of the valence band do not solely arise from silicon 3*s* states. The contributions from platinum 5*d* states almost have the same magnitude. The Greek letters are a tentative assignment of interband transitions; compare Fig. 11.

$$\Delta n = n_{\mathrm{SCF}}^{\mathrm{val}} - n_{\mathrm{atom}}^{\mathrm{val}}. \quad (2)$$

We start the discussion with the familiar cases of a covalent (Si) and a metallic (Pt) crystal in order to compare with the results obtained for silicides. Figure 8(a) presents $\Delta n$ for Pt in a plane perpendicular to the [100] direction (in units of $10^{-3}$ $e^-$/unit volume). Figure 8(b) shows $\Delta n$ for Si in a plane perpendicular to the [110] direction. All indicated atoms are located on the plane of the plot.

Pt shows a rather uniformly increased charge density between 1.5 and 6 m$e^-$/Å$^3$ over the entire interstitial region between the atoms. This area is easily identified as the three highest sections of $\Delta n$ in the plot. Only a small charge accumulation directly between two adjacent atoms is apparent in addition to the uniform isotropic enhancement. At the atomic sites we find the charge density to be decreased. These regions of negative density difference clearly have the form of an atomic *d* orbital. For Si we notice a large localized charge accumulation which corresponds to covalent bonds between neighboring atoms. The charge increase piles up very rapidly from 2 to 20 m$e^-$/Å. In the rest of the interstitial region $\Delta n$ is very small but slightly negative. Our results here are in good agreement with the literature.[12]

Figure 9 displays the valence-charge-density difference $\Delta n$ of PtSi in a [001] plane. The indicated atoms are on the plane of the figure. We find a charge accumulation in the range from 5 to 15 m$e^-$/Å$^3$ along the line between Pt and Si atoms. This localized increase in charge indicates the formation of the covalent bond between these three atoms, which in Ref. 12 is interpreted as the formation of three-center bonds. Unlike the case of purely covalent Si, where $\Delta n$ is positive only directly in between bond partners, we find positive values of $\Delta n$ between 0 and 5 m$e^-$/Å$^3$ in other parts of the interstitial region in PtSi, indicating its partially metallic character.

The charge-density differences for $Pt_2Si$ are shown in Fig. 10 in a [010] plane (a) and in a [001] plane (b). In (a) we notice charge accumulations between, respectively, one Si atom and two Pt atoms, very similar to the case of PtSi. The charge density *n* is increased by values between 3 and

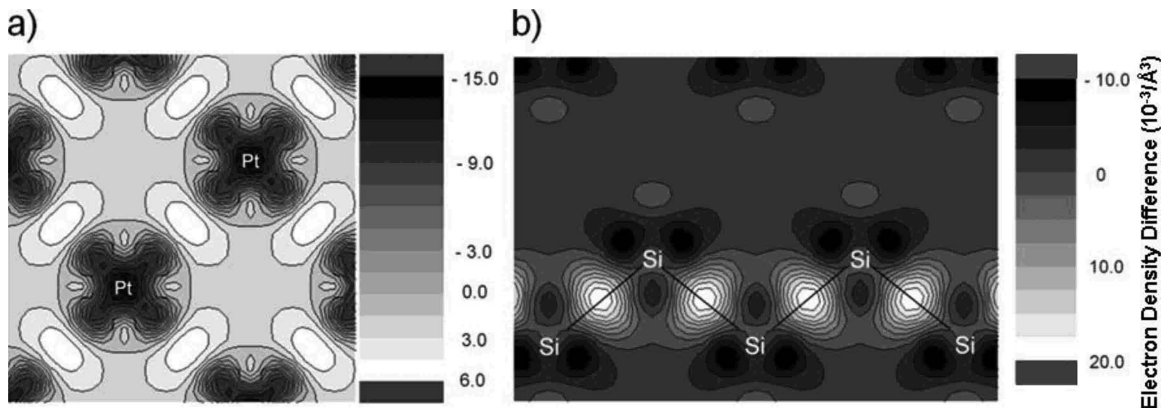


FIG. 8. Superpositions of free atomic valence charge densities subtracted from the fully self-consistent valence charge densities for (a) Pt in the fcc phase and (b) Si in the cubic diamond phase. The plot layer is perpendicular to the [001] direction in (a) and to the [110] direction in (b). The units are m$e^-$/Å$^3$. The scales of the plots are given by the scale bars at the right side of each figure.

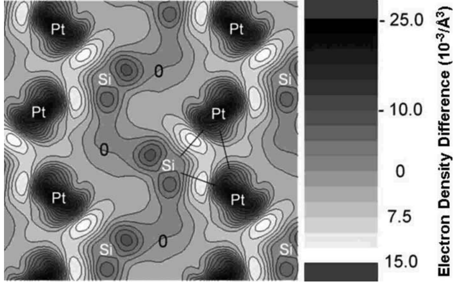


FIG. 9. Superposition of free atomic valence charge densities subtracted from the fully self-consistent valence charge densities for PtSi. The units are m$e^-/\text{Å}^3$. The scale of the contours is given by the scale bar at the right-hand side of contour plot. Indicated atoms are located in the plot layer that is perpendicular to the [001] direction. For convenience some zero contour lines are labeled in the plot.

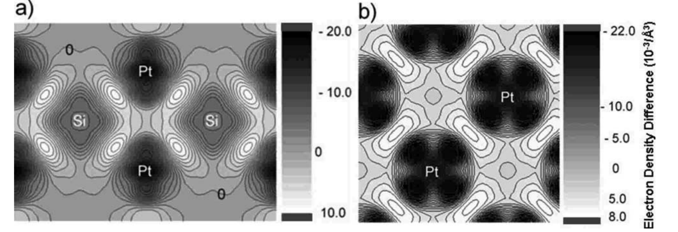


FIG. 10. Superpositions of free atomic valence charge densities subtracted from the fully self-consistent valence charge densities for $Pt_2Si$. In (a) the plot layer is perpendicular to the [010] direction. In (b) the metallic layer perpendicular to the [001] direction is shown, which solely contains Pt atoms. The units are m$e^-/\text{Å}^3$. The scales of the contours are given by the scale bars at the right-hand side of each contour plot. Indicated atoms are located in the plot layer.

10 m$e^-/\text{Å}^3$. We again interpret this as the formation of three-center bonds. Figure 10(b) shows $\Delta n$ in a layer in which only Pt atoms but no Si atoms are located. Not surprisingly the plot clearly resembles Fig. 8(a), where $\Delta n$ of pure Pt is shown. Over the entire interstitial region $n$ is increased by values between 3 and 8 m$e^-/\text{Å}^3$. Thus, on this plane the bonding is clearly metallic. We conclude that, in addition to the poor metallic properties of PtSi and $Pt_2Si$ as captured by their DOSs, their bonding properties indicate a partially covalent character, which as we shall show plays an important role in surface reconstruction.

### D. Optical properties

In Fig. 11 we present the calculated imaginary part $\varepsilon_2$ of the complex dielectric function of $Pt_2Si$ and PtSi. In both cases $\varepsilon_2$ goes to positive infinity for small energies due to the empirical Drude contribution. At higher energies additional structure due to interband transitions is found in the plots. $\varepsilon_2$ of PtSi shows peaks at 1.7 eV ($\alpha$) and 2.95 eV ($\beta$) and a plateau between 4 and 5 eV ($\gamma$). For $Pt_2Si$ a peak at 4.6 eV ($\delta$) is apparent. Similar features, although less distinctive, are found in the experimental data presented in Figs. 3(a) and 3(b). It would be desirable to perform ellipsometry measurements at low temperatures (where phonon scattering is reduced) for better comparison with the electronic band structure. Especially the peaks $\alpha$ and $\beta$ are in good agreement with the experiment. The transitions between occupied and unoccupied states mainly occur between Pt 5$d$ states which can be seen in the state-resolved DOS (PDOS) displayed in Fig. 7. It is quite apparent that the dielectric function of $Pt_2Si$ of much more Drude type (more metallic) than that of PtSi, in agreement with the bonding character discussed above.

## V. SURFACE ENERGIES AND WORK FUNCTIONS OF PtSi

### A. Surface energy of PtSi

We calculated the surface energies for the (011), (110), (020), (101), (100), (010), (112), (001), (310), (130), (211), (121), and (111) orientations of bulk PtSi. Surfaces are simulated within slab geometries, employing supercells that incorporate bulk and vacuum slabs of sufficient thickness. For all orientations the slabs are based on $(1\times1)$ geometries and more complicated reconstructions were not considered. $4\times4\times1$ $k$-point grids are used.

The surface energy of a PtSi is estimated using the Gibbs free-energy approach.[24,25] This method allows for comparison of atomic structures containing different numbers of atoms and is suitable if more than one atomic species is considered. The surface free energy is given by

$$E=\frac{1}{2A}(E_{\text{Slab}}-N_{\text{Si}}E_{\text{Si}}-N_{\text{Pt}}E_{\text{Pt}}-N_{\text{Si}}\mu_{\text{Si}}-N_{\text{Pt}}\mu_{\text{Pt}}). \quad (3)$$

Here the surface energy is given per unit area. $E_{\text{Slab}}$ is the total energy obtained in the supercell calculation. $N_{\text{Si}}$ and $N_{\text{Pt}}$ are the numbers of Si and Pt atoms in the supercell. $E_{\text{Si}}$ and $E_{\text{Pt}}$ are the bulk energies per atom in Si and Pt. $\mu_{\text{Si}}$ and $\mu_{\text{Pt}}$ are the chemical potentials of Si and Pt.

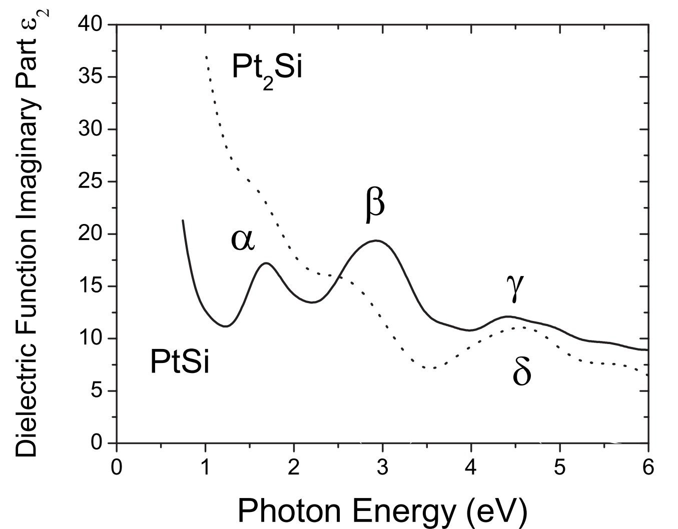


FIG. 11. Calculated imaginary parts of the complex dielectric functions of $Pt_2Si$ and PtSi. We find good qualitative agreement with the experimental data on the pseudodielectric functions presented in Figs. 3(a) and 3(b). Common features in experiment and theory are indicated by Greek letters.

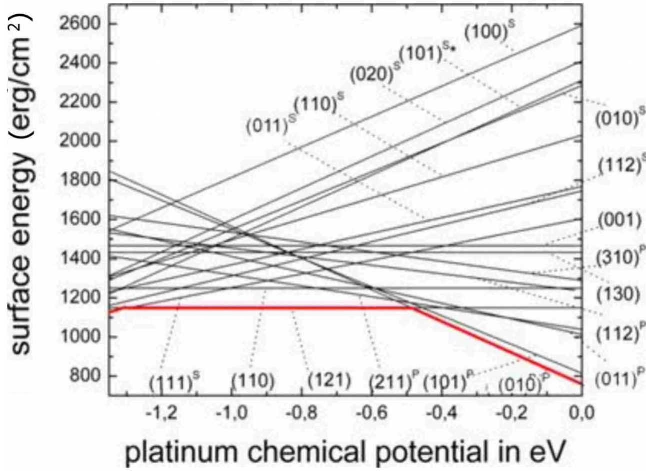


FIG. 12. (Color online) Surface energies of PtSi surfaces for various orientations and terminations as a function of the Pt chemical potential. The chemical potential varies between silicon-rich conditions (left-hand side, $\mu_{Pt}=-1.35$ eV) and platinum-rich conditions (right-hand side, $\mu_{Pt}=0$ eV). For the (101) Si termination (marked with a star), we use the energy of the reconstructed surface (see text).

We previously employed the definition in Eq. (3) and showed that under equilibrium conditions the surface energy can be written as

$$E = \frac{1}{2A}[E_{\rm Slab} - N_{\rm Si}E_{\rm Si} - N_{\rm Pt}E_{\rm Pt} - 2N_{\rm Si}\Delta H_f + \mu_{\rm Pt}(N_{\rm Si} - N_{\rm Pt})]. \tag{4}$$

Here the chemical potentials are measured with respect to their bulk values ($\mu_X^{\rm bulk}=0$). The platinum chemical potential $\mu_{Pt}$ in Eq. (4) is restricted to the energy range

$$2\Delta H_f \le \mu_{\rm Pt} \le 0. \tag{5}$$

$2\Delta H_f$ is the formation energy of a molecular unit in bulk PtSi and we know this number from our bulk investigation (see Table I).

The surface energies of different orientations and terminations are given in Fig. 12 as a function of $\mu_{\rm Pt}$. The superscripts s (p) indicate Si-terminated (Pt-terminated) surfaces. No superscripts are used for stoichiometric surfaces. The zero value of $\mu_{\rm Pt}$ corresponds to Pt-rich conditions, while its lower boundary of $\mu_{\rm Pt}=-1.34$ eV corresponds to Si-rich conditions. Please note that the energy of stoichiometric surfaces is independent of $\mu_{\rm Pt}$. Under Pt-rich conditions the surface energies are spread over a large energy interval from 800 to 2600 erg/cm$^2$, while under Si-rich conditions all surface energies lay between 1100 and 1850 erg/cm$^2$. We find that under a broad range of $\mu_{\rm Pt}$ between $-0.6$ and $-1.1$ eV, the stoichiometric (121) surface exhibits the lowest surface energy. Above $-0.5$ eV the Pt-terminated (010) and (101) surfaces are stabilized. Note that unlike the case of its sister compound PtGe,[26] the semiconductor-terminated surface of PtSi can be stabilized only under extreme Pt-poor conditions.

TABLE III. Work functions of PtSi for various orientations and terminations.

| Surface | Work function (eV) | Surface | Work function (eV) |
|---|---|---|---|
| (020), Si | 4.96 | (310), Pt | 4.68 |
| (011), Si | 4.72 | (101), Pt | 4.97 |
| (110), Si | 4.47 | (112), Pt | 4.86 |
| (010), Si | 4.97 | (121) | 5.01 |
| (100), Si | 4.77 | (110) | 4.96 |
| (101), Si | 4.64 | (001) | 4.93 |
| (111), Si | 4.82 | (130) | 4.96 |
| (010), Pt | 5.15 | | |
| (011), Pt | 4.86 | | |
| (211), Pt | 4.97 | | |

In the x-ray-diffraction pattern given in Fig. 2, the (121) peak clearly is distinctively higher than all other peaks with about 450 counts. In the range between 100 and 200 counts, we find the (110), (101), (111), (220), and (020) peaks. We note that the (121) orientation is the lowest-energy surface and at the same time is the predominant orientation in the PtSi film. The (110) orientation, which has the second lowest surface energy, is also present in the x-ray spectrum by means of the (110) and the (220) peaks. Thus, there appears to be a relation between the preferred crystal-growth directions and the surface energies of PtSi. Consequently, besides kinetics, thermodynamics also seems to play some role in the silicide formation, suggesting the possibility of a controlled silicide growth. The silicide growth of transition metal with atomic numbers close to those of silver and gold is typically dominated by diffusion-controlled kinetics.[27] However, in thin layers the situation is more complicated and the local atomic relaxation may constitute the main part of the rate-control mechanism. We are currently investigating stress accommodation at the Si/silicide interface. The results of this investigation will be presented elsewhere.

### B. Work functions for different PtSi surface orientations and terminations

Employing the DFT-GGA formalism, the work function can be easily determined in slab geometry as $\varphi_m=E_F-E_{\rm Vac}$. Here $E_{\rm Vac}$ and $E_F$ are the vacuum energy and the Fermi level. The vacuum energy $E_{\rm Vac}$ is assessed by using the value of the total electrostatic potential in the vacuum slab of the supercell. The exchange potential can be ignored in the middle of the vacuum region since its true value is zero.

We calculate work functions for different surface orientations and terminations of PtSi listed in Table III. The highest $\varphi_m$ value of 5.15 eV is found for the Pt-terminated (010) surface and the lowest value of 4.47 eV is for the Si-terminated (110) surface. They differ by 0.68 eV. Overall the Si-terminated surfaces tend to have lower work functions than the metal-rich or the stoichiometric surfaces. However, a clear systematic trend cannot be observed. The important stoichiometric low-energy surfaces (121) and (110) have

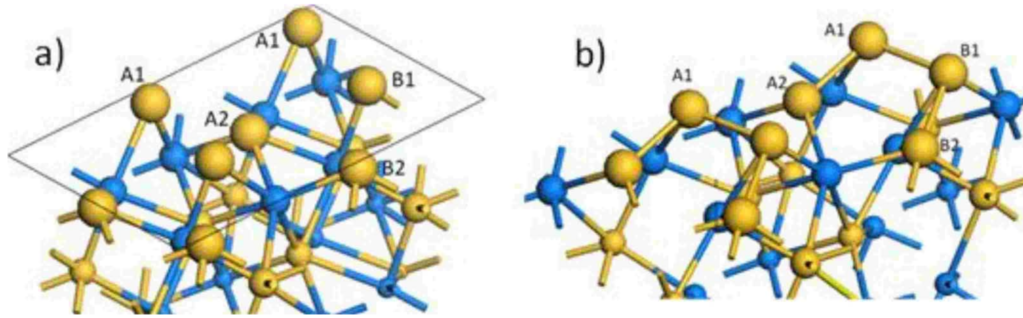


FIG. 13. (Color online) (a) View of the unrelaxed (101) Si-terminated surface of PtSi. A $2\times1$ cell is displayed. The lattice constants of the unit cell are 7.00 and 5.65 Å. The four Si atoms per unit cell in the top layer are represented by the large light balls and are labeled. Pt atoms have dark color. The two Si atoms A1 and B1 are located 1.03 Å above the Si atoms A2 and B2 and they are twofold coordinated. The distance between atoms A1 and B1 is 3.46 Å. (b) View of the reconstructed (101) Si-terminated surface of PtSi. A $2\times1$ unit cell is displayed. Three dimerizations per unit cell can be observed resulting in one tetramer in each unit cell. The bond lengths of the dimers are 2.33 Å between atoms A1 and A2, 2.38 Å between A1 and B1, and 2.44 Å between B1 and B2. Two back bonds between atoms A1 and A2 to lower Pt atoms are broken during the relaxation.

work functions of 5.01 and 4.96 eV, respectively. Several surfaces have work functions very close to these two values. Hence, we expect experimental studies will report values of 4.9–5.0 eV. To gauge the reliability of our calculation, we determine the work functions of Ni(111) and Pt(111) to 5.09 and 5.70 eV. The experimental values for these surfaces are 5.35 eV (Ref. 28) and 5.70 eV,[29] respectively.

### C. Reconstruction of the (101) surface

As we have pointed out in the discussion above, the bonding of bulk PtSi shows a strongly covalent character. From this perspective it would seem likely that PtSi surfaces tend to reconstruct in a manner similar to how semiconductor surfaces reconstruct. However, metal surfaces usually do not reconstruct with the notable exception of Au. Thus, the very nature of reconstructions on PtSi surfaces (or in general on transition-metal silicide surfaces) is of fundamental interest. Previously, we reported on a possible reconstruction of a NiGe surface.[26] We found that the formation of bonds between Ge atoms causes a significant decrease in the surface energy and is about 50% of the bulk cohesive energy per bond in Ge.

To study this issue, we now discuss in more details the (101) Si-terminated surface. The unrelaxed surface is displayed in Fig. 13(a). Four Si atoms are located in the first layer. They are labeled A1, B1, A2, and B2. Atoms A1 and B1 are located 1.03 Å above atoms A2 and B2. They are followed by four Pt atoms in the second layer. Considering the findings in Secs. IV B and IV C, one can imagine the two uppermost Si atoms A1 and B1 as twofold coordinated via back bonds to Pt atoms in the second layer. Atoms A1 and B1 are separated by 3.46 Å, which is comparable to the second-nearest-neighbor distance in bulk Si of 3.84 Å. Hence, the unrelaxed surface vaguely resembles the Si(100) surface. The reconstruction we find, however, is more complicated and is shown in Fig. 13(b). Overall we see three additional Si-Si dimers forming on the surface with bond lengths ranging between 2.33 and 2.44 Å, resulting in one tetramer in each surface unit cell. These should be compared to the nearest-neighbor distance in bulk Si of 2.34 Å (a theoretical value). The tetramers can be clearly identified in Fig. 14 where we display the valence charge density in the surface layer. In addition, during the reconstruction two back bonds to lower Pt atoms break. The total energy gain from the reconstruction when compared to a simple relaxation is 0.84 eV per surface unit cell or 0.33 $J/m^2$. This is a large value and amounts to 37% of the Si bulk cohesive energy per bond. It is comparable to typical energy gains due to reconstructions on semiconductor surfaces.[30] However, as can be seen in Fig. 12 this is not enough to stabilize this termination. Even under Si-rich conditions it is about 0.1 $J/m^2$ higher in energy than the Si-terminated (111) surface.

## VI. CONCLUSIONS

We have investigated the electronic structure of the two silicide phases PtSi and $Pt_2Si$ from first principles. The bonding is found to have a strongly covalent character, in good

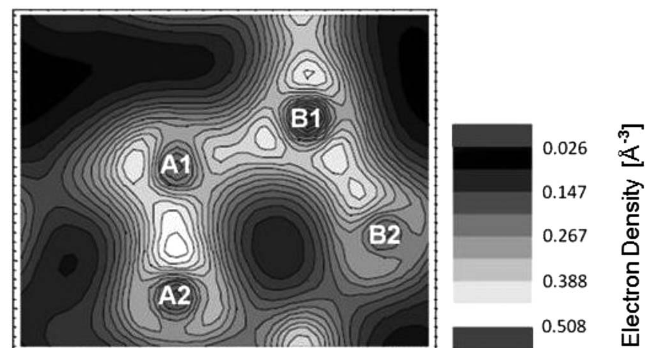


FIG. 14. Valence charge density averaged over approximately 1 Å within the first surface layer of the reconstructed PtSi(101) surface. The atoms are labeled as in Fig. 13. The scale bar at the right-hand side of the plot gives the values of the contour lines. The units are $e^-/\text{Å}^3$. The tetramer that occurs after the reconstruction can be clearly identified by means of the increased charge density in between the respective atoms.

agreement with previous results. As a consequence PtSi surfaces are able to reconstruct with significant energy gains comparable to those of semiconductor surfaces. We have presented a detailed study of the surface thermodynamics of PtSi. In particular, we find the stoichiometric (121) surface to have the lowest energy over a wide range of growth conditions, especially under the estimated growth conditions. This orientation corresponds to the highest peak in our x-ray-diffraction data, suggesting that thermodynamics plays an important role in silicide formation. We have calculated the work function of PtSi as a function of the surface orientation and stoichiometry, extending our previous results to Pt-rich surfaces. We have also measured the complex dielectric function of the two silicide phases PtSi and $Pt_2Si$ in the range from 0.75 to 6.5 eV during the annealing process of a thin silicide film. The absorption coefficient of PtSi exhibits non-Drude peaks due to interband transitions. Using first-principles calculations, we have identified these transitions with the 5$d$ manifold of platinum. In this paper we have not attempted to model the Si/PtSi interface explicitly, and our theoretical results should be interpreted with caution when applied to the real interface. However, we believe the results further our understanding of the experimental data, and hope they will inspire more atomic-resolution electron-microscopy studies of this important materials system.

## ACKNOWLEDGMENTS

We thank Manish Niranjan and Len Kleinman for insightful discussions. This work was supported by the Semiconductor Research Corporation under Contract No. 2006-JV-1439 and Texas Advanced Computing Center (TACC).

*demkov@physics.utexas.edu

[1] S. Zhang and M. Ostling, CRC Crit. Rev. Solid State Mater. Sci. **28**, 1 (2003).
[2] C. Detavernier, A. S. Özcan, J. Jordan-Sweet, E. A. Stach, J. Tersoff, F. M. Ross, and C. Lavoie, Nature (London) **426**, 641 (2003).
[3] C. Detavernier and C. Lavoie, Appl. Phys. Lett. **84**, 3549 (2004).
[4] W. J. Taylor, M. J. Rendon, E. Verret, J. Jiang, C. Capasso, D. Sing, J. Y. Nguyen, J. Smith, E. Luckowski, A. Martinez, J. Schaeffer, and P. Tobin, in *Silicon Front-End Junction Formation–Physics and Technology*, MRS Symposia Proceedings No. 810, edited by P. Pichler, A. Claverie, R. Lindsay, M. Orlowski, and W. Windl (Materials Research Society, Warrendale, PA, 2004), p. C1.1.
[5] J. Iwai, T. Ohguro, and S. Ohmi, Microelectron. Eng. **60**, 157 (2002).
[6] M. K. Niranjan, S. Zollner, L. Kleinman, and A. A. Demkov, Phys. Rev. B **73**, 195332 (2006).
[7] V. W. Chin, M. A. Green, and J. W. V. Storey, Solid-State Electron. **36**, 1107 (1993).
[8] S. Zollner, in *2007 International Conference on Frontiers of Characterization and Metrology*, AIP Conf. Proc. No. 931, edited by D. G. Seiler, A. C. Diebold, R. McDonald, M. C. Garner, D. Herr, R. P. Khosla, and E. M. Secula (AIP, Melville, NY, 2007), p. 337.
[9] S. Zollner, P. Grudowski, A. Thean, D. Jawarani, G. Karve, T. White, S. Bolton, H. Desjardins, M. Chowdhury, K. Chang, M. Jahanbani, R. Noble, L. Lovejoy, M. Rossow, D. Denning, D. Goedeke, S. Filipiak, R. Garcia, M. Raymond, V. Dhandapani, D. Zhang, L. Kang, P. Crabtree, X. Zhu, M. L. Kottke, R. Gregory, P. Fejes, X.-D. Wang, D. Theodore, W. J. Taylor, and B.-Y. Nguyen, Proceedings of the 2007 IEEE International SOI Conference, Indian Wells, California (unpublished), p. 75.
[10] O. Beckstein, J. E. Klepeis, G. L. W. Hart, and O. Pankratov, Phys. Rev. B **63**, 134112 (2001).
[11] N. Franco, J. E. Klepeis, C. Bostedt, T. Van Buuren, C. Heske, O. Pankratov, T. A. Callcott, D. L. Ederer, and L. J. Terminello, Phys. Rev. B **68**, 045116 (2003).
[12] J. E. Klepeis, O. Beckstein, O. Pankratov, and G. L. W. Hart, Phys. Rev. B **64**, 155110 (2001).
[13] C. Kumpf, R. Nicula, and E. Burkel, J. Appl. Crystallogr. **30**, 1016 (1997).
[14] T. Stark, H. Grünleitner, M. Hundhausen, and L. Ley, Thin Solid Films **358**, 73 (2000).
[15] G. Kresse and J. Furthmüller, Phys. Rev. B **54**, 11169 (1996); G. Kresse and J. Hafner, *ibid.* **47**, R558 (1993).
[16] P. E. Blöchl, Phys. Rev. B **50**, 17953 (1994).
[17] G. Kresse and D. Joubert, Phys. Rev. B **59**, 1758 (1999).
[18] J. P. Perdew, K. Burke, and M. Ernzerhof, Phys. Rev. Lett. **77**, 3865 (1996).
[19] M. D. Segall, P. J. D. Lindan, M. J. Probert, C. J. Pickard, P. J. Hasnip, S. J. Clark, and M. C. Payne, J. Phys.: Condens. Matter **14**, 2717 (2002).
[20] M. P. Marder, *Condensed Matter Physics* (Wiley, New York, 2000).
[21] E. J. Graeber, R. J. Baughman, and B. Morossin, Acta Crystallogr. **29**, 1991 (1973).
[22] R. P. Ram and S. Bhan, Z. Metallkd. **69**, 524 (1978).
[23] C. Kittel, *Introduction to Solid State Physics*, 6th ed. (Wiley, New York, 1986).
[24] J. Padilla and D. Vanderbilt, Surf. Sci. **418**, 64 (1998).
[25] G. X. Qian, R. M. Martin, and D. J. Chadi, Phys. Rev. B **38**, 7649 (1988).
[26] M. K. Niranjan, L. Kleinman, and A. A. Demkov, Phys. Rev. B **75**, 085326 (2007).
[27] F. M. d'Huerle and P. Gas, J. Mater. Res. **1**, 205 (1986).
[28] B. G. Baker, B. B. Johnson, and G. L. C. Maire, Surf. Sci. **24**, 572 (1971).
[29] M. Kiskinova, G. Pirug, and H. P. Bonzel, Surf. Sci. **133**, 321 (1983).
[30] I. Larkin and A. Vagov, Phys. Rev. B **67**, 115318 (2003).